Discrete Element Modeling of a fault reveals that viscous rolling relaxation controls friction weakening

Alexandre Sac–Morane[1,2*], Manolis Veveakis[1†] and Hadrien Rattez[2†]

[1*]Multiphysics Geomechanics Lab, Duke University, Hudson Hall Annex, Room No. 053A, Durham, 27708, NC, USA.
[2]Institute of Mechanics, Materials and Civil Engineering, UCLouvain, Place du Levant 1, Louvain-la-Neuve, 1348, Belgium.

*Corresponding author. E-mail: alexandre.sacmorane@duke.edu;
Contributing authors: manolis.veveakis@duke.edu;
hadrien.rattez@uclouvain.be;
†These authors contributed equally to this work.

Abstract

In this paper, the effect of the rolling and damping values on the macro friction coefficient have been investigated. The introduction of the viscous rolling relaxation induces a friction weakening. Hence, it has been highlighted that this element can act against the angular spring and decreases the sample stiffness. This influence must be considered to not overestimate the toughness of a fault.

Keywords: Discrete element method, Rolling parameter, Fault friction, Granular materials

1 Introduction

If the focus is made on the damage slip zone of a fault, it appears the rock mass is pulverized and can be considered as a granular material [1], [2]. The global behavior observed at the macro scale is a result of interactions at the micro-scale.

The Discrete Element Method has been designed to consider those interactions between grains [3]. Even if the simplest model is a linear one [4], [5], contact laws can be easily modified [6]: (i) considering the grain crushing [7], [8], (ii) investigating the effect of the pressure solution [9], [10], [11], (iii) exploring the effect of the healing [12], [13], (iv) appreciating the influence of the cohesion in the matter [14], [15], [16] or (v) the cohesion induced by the pore fluid [17], [18] for examples. Also, it allows some to focus on the temperature influence. Hence, it appears the pressurization of the pore fluid [19], [20] and the melting [21], [22] are main phenomena during large crustal events.

Our work is motivated by previous experiments made on antigorite [23]. The main goal is to assess the influence on global behavior of contact laws and parameters values. Even if different relevant outputs for dense granular flows are reviewed by the French research group *Groupement de Recherche Milieux Divisés* (GDR MiDi) [24], we are focused in this paper on the macro friction coefficient at steady state.

We are going to explore the influence of the rolling resistance model. Experimental results [25], [26], and numerical ones [27], [28], [29] have highlighted that grains rolling has a real impact on the sample behavior. A lot of rolling models have been formulated [30], [31]. But it appears the most accurate is an elastic-plastic spring dashpot model [32], [33]. From this formulation, a lot of investigations have been done about the angular spring parameter. For examples: (i) the rolling helps the formation of shear bands and decrease the sample strength [34], [35], [36], [37] or (ii) the stress-dilatancy curves are modified [38], [39], [40], [41]. It appears that the rolling resistance comes from friction [42], [43] and roughness [44], [45], [46]. Even if superquadric particles allow to approximate the shape, those simulations represent an enormous computational cost. Because of this fact, some geometric laws about the rolling friction have been developed [47], [48]. Thanks to that simulations can keep using round particles with a rolling resistance (from an equivalent shape).

On other hand, the angular damping influence is not well known. Hence, it is not considered in most of the DEM simulations. It appears this parameter is used more for stability reasons [30], [32] than physical meaning. Nevertheless, Jiang has formulated a link between the rolling and the normal dampings [49]. But it was under the assumption of a geometrically derived kinematical model.

We decided to realize in this paper a parametric study over the rolling and the damping parameters to understand better their influence on the macro friction coefficient of a shearing fault.

2 Theory and formulation

The Discrete Element Model (DEM) is an approach developed by Cundall & Strack [3] to simulate granular materials at the particles level. The foundation of this method is to consider inside the material the individual particles and their interactions explicitly. Newton's laws defined at equations 1 and 2 help to compute the motion of the grain.

$$m\frac{\partial v_i}{\partial t} = m \times g_i + \sum f_i \tag{1}$$

$$I \times \rho\frac{\partial \omega_i}{\partial t} = \sum \epsilon_{ijk} f_j R_k + \sum M_i \tag{2}$$

where m is the particle mass, I the moment of inertia, g is the gravity acceleration, f the contact forces, M the contact moments, r the radius.

Considering two particles with radii R^1 and R^2, the interaction between particles is computed only if the distance δ between grains verifies equation 3.

$$\delta < R^1 + R^2 \tag{3}$$

Once contact is detected between grains 1 and 2, interactions (force and moment) are computed from relative motions Δu and $\Delta\omega$ with equations 4 and 5.

$$\Delta u_i = u_i^1 - u_i^2 + \epsilon_{ijk}\left(r_j^1\theta_k^1 - r_j^2\theta_k^2\right) \tag{4}$$

$$\Delta\omega_i = \omega_i^1 - \omega_i^2 \tag{5}$$

where u is the particle displacement, θ the angular displacement and ω the angular velocity of the grain.

The contact models between cohesionless particles obey the Hertz contact theory [50]. Normal, tangential and rolling models are shown at figure 1 and formulated at equations 6 and 7. Some details about Hertz laws are given at equation 8. A lot of rolling models could be applied to our case but we decide to use an elastic-plastic spring-dashpot model because it is the most accurate choice [30].

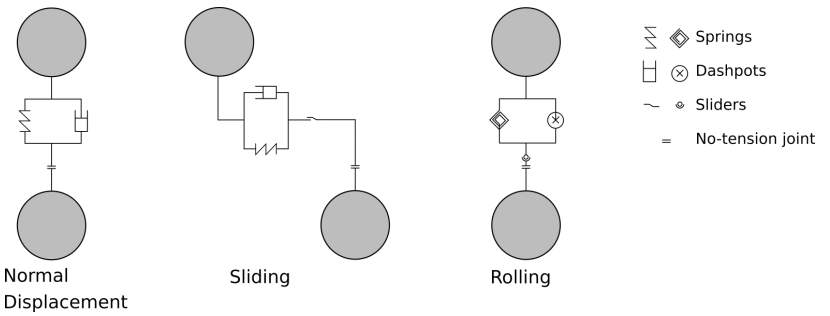

Fig. 1 The contact between two particles obeys to normal, tangential and rolling elastic-plastic spring-dashpot laws.

$$\begin{aligned} f &= f_n + f_t \\ f_n &= k_n\Delta_n - \gamma_n v_n \quad \text{The normal force} \\ f_t &= k_t\Delta_t - \gamma_t v_t \quad \text{The tangentiel force} \\ f_t &\leq \mu_p f_n \end{aligned} \tag{6}$$

The tangential displacement Δ_t is computed by integrating the relative tangential velocity at the contact point over time.

$$\begin{aligned} M &= M^k + M^d \\ M^k_{t+\Delta t} &= M^k_t - k_r \Delta\theta_r \\ \mathsf{M\hat{}k\_t{+}\Delta t''} &\leq M^m = \mu_r R^* f_n \\ M^d_{t+\Delta t} &= \begin{cases} -C_r\dot{\theta_r} & \text{if } \mathsf{M\hat{}k\_t{+}\Delta t''} < M^m \\ 0 & \text{if } \mathsf{M\hat{}k\_t{+}\Delta t''} = M^m \end{cases} \end{aligned} \tag{7}$$

$$\begin{aligned} k_n &= \tfrac{4}{3} Y^* \sqrt{R^* \Delta_n} \\ \gamma_n &= -2\sqrt{\tfrac{5}{6}}\beta\sqrt{S_n m^*} \geq 0 \\ k_t &= 8 G^* \sqrt{R^* \Delta_n} \\ \gamma_t &= -2\sqrt{\tfrac{5}{6}}\beta\sqrt{S_t m^*} \geq 0 \\ S_n &= 2 Y^* \sqrt{R^* \Delta_n} \\ S_t &= 8 G^* \sqrt{R^* \Delta_n} \\ \beta &= \frac{ln(e)}{\sqrt{ln^2(e)+\pi^2}} \\ \frac{1}{Y^*} &= \frac{1-{\nu^1}^2}{Y^1} + \frac{1-{\nu^2}^2}{Y^2} \\ \frac{1}{G^*} &= \frac{2(2-\nu^1)(1+\nu^1)}{Y^1} + \frac{2(2-\nu^2)(1+\nu^2)}{Y^2} \\ \frac{1}{R^*} &= \frac{1}{R^1} + \frac{1}{R^2} \\ \frac{1}{m^*} &= \frac{1}{m^1} + \frac{1}{m^2} \\ k_r &= 2,25 k_n \mu_r^2 R^{*2} \\ C_r &= \eta_r C_r^{crit} \\ C_r^{crit} &= 2\sqrt{I_r k_r} \\ I_r &= \left(\frac{1}{I^1 + m^1 {R^1}^2} + \frac{1}{I^2 + m^2 {R^2}^2} \right)^{-1} \end{aligned} \tag{8}$$

3 Numerical model

The simulation setup is illustrated at figure 2. The box is a $0,004\,m \times 0,006\,m \times 0,0024\,m$ region. Faces x and z are under periodic conditions. The gravity is not considered because its effect stays negligible under the vertical pressure applied.

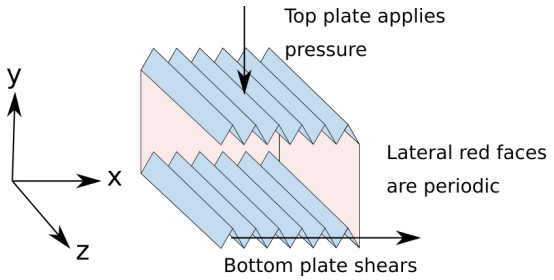

Fig. 2 The simulation box with triangle plates and periodic faces.

The simulation, made by the open-source software LIGGGHTS [51], is in several steps illustrated at figure 3:

1. The box, bottom and top triangle plates are created.
2. 2500 particles are generated following the distribution presented in table 1 equivalent to the one used by Morgan [13].
3. Top plate applies vertical stress of 10 MPa by moving following the y axis. This plate is free to move vertically to verify this confining and allow volume change.
4. The sample is sheared by moving the bottom plate at the speed of 100 μm/s until 100% strain. This step is then repeated at the speed of 300 and 1000 μm/s.

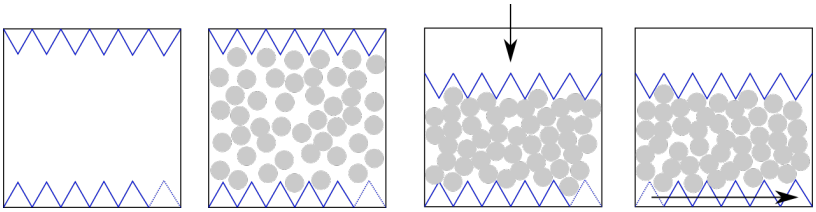

Fig. 3 The simulation is in multiple steps : creation of the box and particles, application of the normal force and shearing.

Radius	Percentage	Number of particles
R1 = 0, 2 *mm*	14%	2500
R2 = 0, 15 *mm*	29%	
R3 = 0, 1 *mm*	57%	

Table 1 Distribution used described by discrete radius, percentage of the mass and total number of grains.

The different parameters needed for the DEM simulation are presented in table 2. We can notice the time step dt must verify the Rayleigh condition [50], [52], [53] defined at equation 9.

$$dt_R = \pi \times r \times \frac{\sqrt{\rho/G}}{0,1631 \times \nu + 0,8766} \tag{9}$$

With every computing test, the main problem is the running time. The time step dt must be selected considering the number of particles, the computing power, the stability of the simulation and the time scale of the test. In our case, we are looking for a 10^2 seconds term [54]. If we include the default value into equation 9 the time step is around 10^{-8} second and the running time skyrockets. To answer this we can easily change the density ρ and the shear modulus G. We will see those parameters are included in two dimensionless numbers defined at the equation 10: the contact stiffness number κ [55], [56], [57] and the inertial number I [24], [56].

Variable	Short Name	Value
Simulation variables		
Time step	dt	$1,5e^{-6}$ s
Height of the sample	h	$0,005$ m
Shear rate	$\gamma' = v_{shear}/h$	$2-6-20\%$
Contact stiffness number	$\kappa = \left(\frac{Y}{P(1-\nu^2)}\right)^{2/3}$	400
Inertial number	$I = \gamma' d\sqrt{\rho/P}$	$10^{-6} - 10^{-5}$
Mechanical variables		
Density	ρ	$2000000\, kg/m^3$
Youngs modulus	Y	$70\, GPa$
Poissons ratio	ν	$0,3$
Restitution coefficient	e	1
Rolling friction coefficient	μ_r	$0-0,25-0,5-0,75-1$
Rolling viscous damping coefficient	η_r	$0-0,25-0,5-0,75$
Friction coefficient	μ_p	$0,5$

Table 2 DEM parameters.

$$\begin{aligned} \kappa &= \left(\frac{Y}{P(1-\nu^2)}\right)^{2/3} \quad \text{The contact stiffness number} \\ I &= \gamma' d_{50}\sqrt{\rho/P} \qquad\qquad\quad \text{The inertial number} \end{aligned} \tag{10}$$

Where $\gamma' = v_{shear}/h$ is the shear rate, h is the height of the sample during the shear and d_{50} the mean diameter.

It appears the constitutive law is sensitive to κ because grains are not rigid enough ($\kappa \leq 10^4$) [55]. By this fact, it becomes not possible to change the Young modulus Y (and so the shear modulus G). The inertial number I represents the behavior of the grains, which can be associated with solids, liquids or gases [58]. This dimensionless parameter does not affect the constitutive law if the flow regime is at critical state ($I \leq 10^{-3}$) [24], [56]. In conclusion, the density ρ can be modified, if we stay under the condition $I \leq 10^{-3}$, to increase the time step and solve our computing problem.

4 Results and discussion

A parametric study has been done on the rolling friction coefficient μ_r and the rolling viscous damping coefficient η_r. As figure 4 shows, the macro friction coefficient is plotted following the shear strain. This coefficient μ is computed by considering $\mu = F_y/F_x$, where F_y (resp. F_x) is the component following the y-axis (resp. x-axis) of the force applied on the top plate. Because of the granular aspect, there is a lot of oscillation. To reduce this noise, at least 3 simulations are run by a set of parameters (μ_r, η_r) and a mean curve is computed. Moreover, only the steady-state is considered and an average value is estimated.

The comparison of the macro friction coefficient with different parameters set is highlighted at figures 5, 6, 7. It appears there is an increase of the

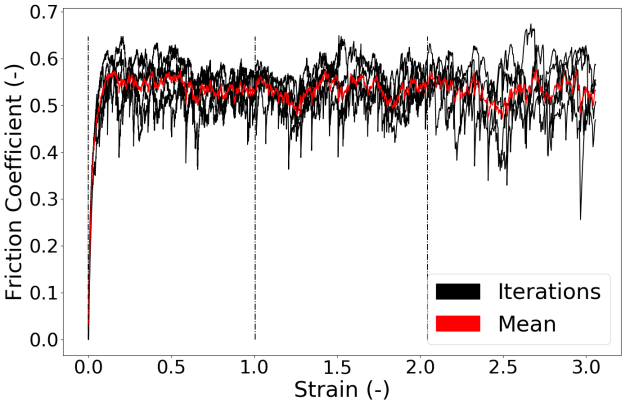

Fig. 4 Example of μ-γ curve (dotted lines mark the different velocity steps 100 - 300 - 1000 μm/s).

fault friction coefficient with the rolling resistance μ_r until a critical point depending on the rolling damping η_r. This reduction of the stiffness with the rolling damping is not easy to understand at the first point. The larger is the damping, the stiffer should be the system. Two main questions should be answered: why does the friction coefficient decrease with the rolling resistance if there is damping? Why is the reduction larger with the damping value?

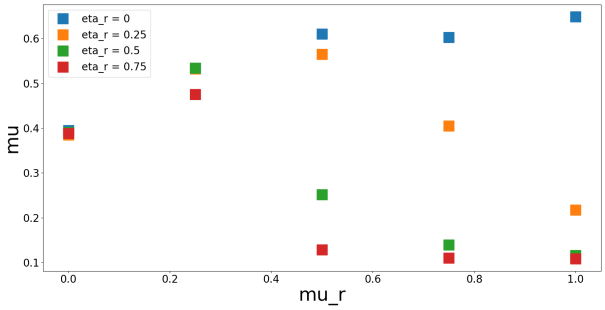

Fig. 5 $v_{shear} = 100\,\mu m/s$

Figures 8, 9, 10, 11 help to understand the behavior. It shows the rotation of particle (in red) during four different cases. We can notice that the fewer rotations there are, the stiffer the system will be. It appears the number of rolling particle increases with the rolling resistance, see figures 8, 9 and 10. The decrease of the friction coefficient is explained by particles rolling. Moreover, it is shown at figures 9 and 11 that damping increases the number of rolling particles and so the friction coefficient is reduced.

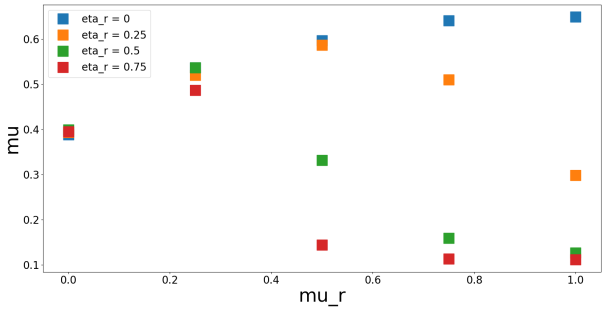

Fig. 6 $v_{shear} = 300\,\mu m/s$

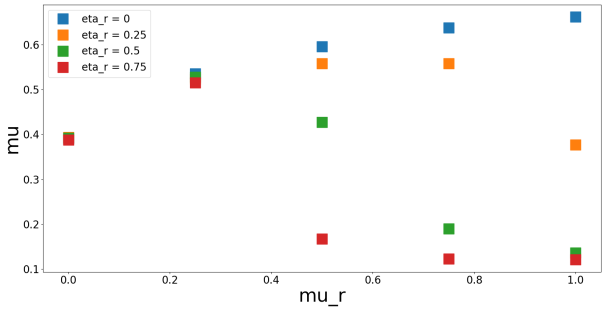

Fig. 7 $v_{shear} = 1000\,\mu m/s$

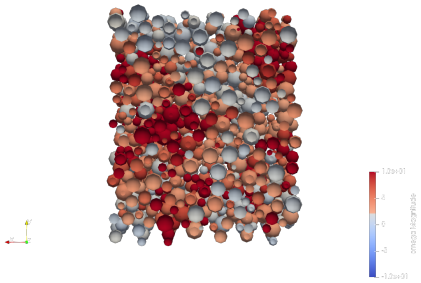

Fig. 8 $\mu_r = 0,25$ and $\eta_r = 0,5$

A focus on the model equations must be done at relation 11 to understand better those observations (the input rolling parameters are emphasized in red). First, it appears the increment of the spring ΔM_r^k depends on μ_r^2 while the plastic limit $\mu_r R^* F_n$ depends only on μ_r. There is a square factor between those values. Thus, this plastic limit, and so grain rolling, is reached easier with a larger rolling resistance μ_r for a same angular displacement θ_r.

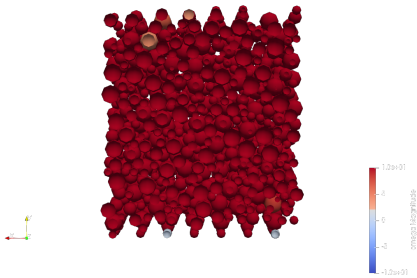

Fig. 9 $\mu_r = 0,50$ and $\eta_r = 0,5$

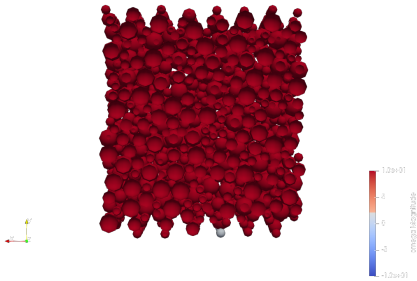

Fig. 10 $\mu_r = 1$ and $\eta_r = 0,5$

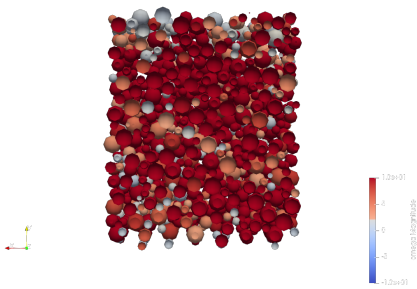

Fig. 11 $\mu_r = 0,5$ and $\eta_r = 0$

$$
\begin{array}{lll}
M_r & = M_r^k + M_r^d & \\
\mathsf{M\hat{}k\_-r,t+}\Delta t'' & \leq \mu_r R^* F_n & \\
\Delta M_r^k & = -2,25 k_n {\mu_r}^2 R^{*2} \Delta\theta_r & \\
M^d_{r,t+\Delta t} & = \begin{cases} -2\eta_r\mu_r\sqrt{2,25 I_r k_n}\dot{\theta}_r & \text{if } \mathsf{M\hat{}k\_-r,t+}\Delta t'' < \mu_r R^* F_n \\ 0 & \text{if } \mathsf{M\hat{}k\_-r,t+}\Delta t'' = \mu_r R^* F_n \end{cases} &
\end{array}
\tag{11}
$$

Concerning the damping, it avoids the variation of the angular position ($\dot{\theta_r} \to 0$) during the elastic phase. As we have seen before, the main part of the sample is at the plastic phase and particles roll. So, it is as the damping acts in opposition of the angular spring, keeping grain into the plastic phase. We can notice that we have decided in this paper to shut down the damping moment when the angular plastic limit is reached (see equation 11).

In this way, we can understand better the reduction of the friction coefficient with the rolling stiffness μ_r if damping is active. We can notice there is no decrease but an increase of the friction coefficient in the case of no damping. In absence of this one, the angular spring can act normally. The larger is the rolling parameter, the stiffer is the global sample.

Figures 12, 13, 14, 15 highlight the shearing speed influence on the system. It is the same results as before but plotted in another way. It appears there is no speed effect visible in most simulations as the friction coefficient keeps the same value. It is not surprising that no speed effects are spotted because there are no other parameters except the damping parameter which depends on speed or time. A speed influence is nevertheless noticed for cases where the friction coefficient starts to decrease with rolling resistance (for example the case $\mu_r = 0,5$ and $\eta_r = 0,5$ at figure 14). As shown at figure 9, few particles (in orange or in white) are still not rolling during this critical step. The damping value is not large enough to cancel the effect of the spring and few grains are in the elastic phase. The damping creates so in this case a speed influence. If the damping value is larger, we have seen particles tend to be all in the plastic phase. If it is lower, the damping is negligible or null. In both cases, the speed effect disappears.

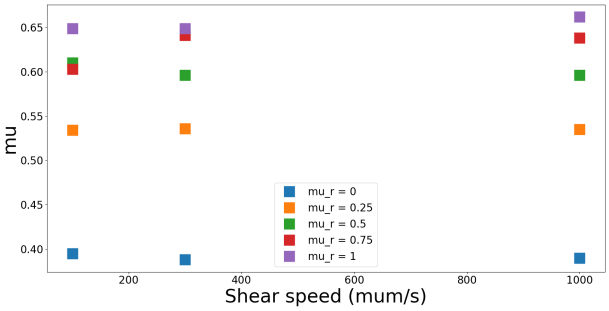

Fig. 12 $\eta_r = 0$

5 Conclusion

In this paper, we have considered granular materials into a plane shear configuration to investigate the effect of the rolling resistance and damping on

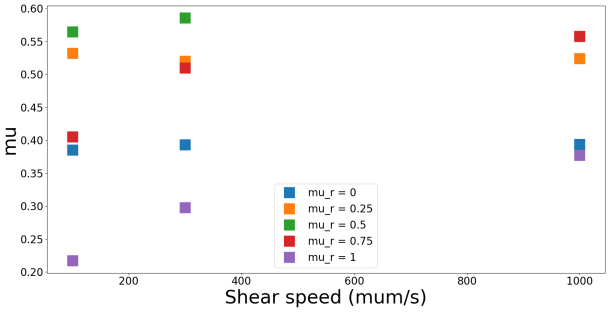

Fig. 13 $\eta_r = 0.25$

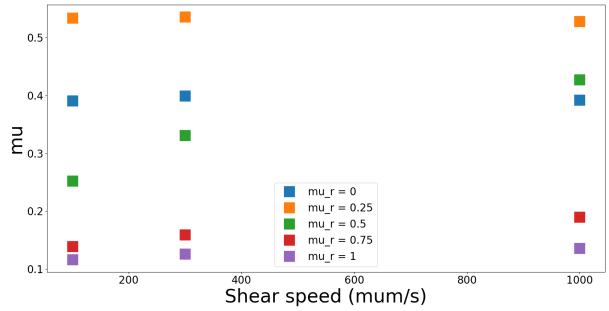

Fig. 14 $\eta_r = 0.5$

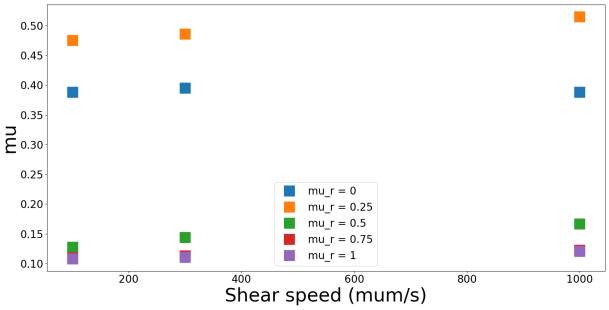

Fig. 15 $\eta_r = 0.75$

the macroscopic friction coefficient. Thank numerical DEM simulations, the relation between those parameters becomes clearer. It appears :

1. In the no damping case, the sample stiffness increases with the rolling resistance.

2. The consideration of the rolling damping introduces a critical point. For a constant damping value, the sample stiffness increases the rolling parameter until this critical point is reached. Then, the stiffness starts to decrease until a residual value. Hence, the damping tend to act against the spring and grains roll.
3. No visible speed effects have been highlighted except at critical point. For the same rolling resistance value : (i) When the damping parameter is not large enough, the angular spring is the main element and no speed dependency is spotted, (ii) when the damping parameter is too large, all grains are in the plastic phase (roll) and the residual value is reached and (iii) when the damping parameter is at critical value, there is no main element in the rolling model, speed dependency occurs.

6 Acknowledgements

Computational resources have been provided by the Consortium des Équipements de Calcul Intensif (CÉCI), funded by the Fonds de la Recherche Scientifique de Belgique (F.R.S.-FNRS) under Grant No. 2.5020.11 and by the Walloon Region.

References

[1] Rodrick Myers and Atilla Aydin (2004) The evolution of faults formed by shearing across joint zones in sandstone. Journal of Structural Geology 26:947-966. https://doi.org/10.1016/j.jsg.2003.07.008

[2] Thomas Poulet and Manolis Veveakis and Marco Herwegh and Thomas Buckingham and Klaus Regenauer-Lieb (2014) Modeling episodic fluid-release events in the ductile carbonates of the Glarus thrust. Geophysical Research Letters 41:7121-7128. https://doi.org/10.1002/2014GL061715

[3] Burman, B. C. and Cundall, P. A. and Strack, O. D.L. (1980) A discrete numerical model for granular assemblies. Geotechnique 30:331-336.https://doi.org/10.1680/geot.1980.30.3.331

[4] Imole, Olukayode I. and Wojtkowski, Mateusz and Magnanimo, Vanessa and Luding, Stefan (2014) Micro-macro correlations and anisotropy in granular assemblies under uniaxial loading and unloading. Phys. Rev. E 89, 042210. https://org.doi/10.1103/PhysRevE.89.042210

[5] González, S. and Windows-Yule, C. R. K. and Luding, S. and Parker, D. J. and Thornton, A. R. (2015) Forced axial segregation in axially inhomogeneous rotating systems. Phys. Rev. E 92, 022202. https://org.doi/10.1103/PhysRevE.92.022202

[6] O'Sullivan, Catherine (2011) Particulate Discrete Element Modelling: A Geomechanics Perspective. CRC Press, London. https://doi.org/10.1201/9781482266498

[7] Kevin J. Hanley and Catherine O'Sullivan and Xin Huang (2015) Particle-scale mechanics of sand crushing in compression and shearing using DEM. Soils and Foundations 55:1100-1112. https://doi.org/10.1016/j.sandf.2015.09.011

[8] Zhang, Ningning and Ciantia, Matteo O. and Arroyo, Marcos and Gens, Antonio (2021) A contact model for rough crushable sand. Soils and Foundations 61: 798-814.https://doi.org/10.1016/j.sandf.2021.03.002

[9] Elliott, D. and Rutter, Ernest (1976) The Kinetics of Rock Deformation by Pressure Solution. Philosophical Transactions of The Royal Society A: Mathematical, Physical and Engineering Sciences 283:218-219. https://doi.org/10.1098/rsta.1976.0079

[10] Florian K. Lehner (1995) A model for intergranular pressure solution in open systems. Tectonophysics 245:153-170. https://doi.org/10.1016/0040-1951(94)00232-X

[11] van den Ende, M. P.A. and Marketos, G. and Niemeijer, A. R. and Spiers, C. J. (2018) Investigating Compaction by Intergranular Pressure Solution Using the Discrete Element Method. Journal of Geophysical Research: Solid Earth 123:107-124. https://doi.org/10.1002/2017JB014440

[12] S., Abe and James H., Dieterich and Peter, Mora and David, Place (2002) Simulation of the influence of rate- and state-dependent friction on the macroscopic behavior of complex fault zones with the lattice solid model. Pure and Applied Geophysics 159:1967-1983. https://doi.org/10.1007/s00024-002-8718-7

[13] Morgan, Julia K. (2004) Particle dynamics simulations of rate- and state-dependent frictional sliding of granular fault gouge. Pure and Applied Geophysics 161:1877-1891. https://doi.org/10.1007/s00024-004-2537-y

[14] Potyondy, David O. and Cundall, P. A. (2004) A bonded-particle model for rock. International Journal of Rock Mechanics and Mining Sciences 41:1329-1364. https://doi.org/10.1016/j.ijrmms.2004.09.011

[15] Li, Xikui and Feng, Yuntian and Mustoe, Graham (2017) Influences of Stiffness Ratio, Friction Coefficient and Strength Ratio on the Macro Behavior of Cemented Sand Based on DEM.In: Li X., Feng Y., Mustoe G. (eds) Proceedings of the 7th International Conference on Discrete Element Methods. DEM 2016. Springer Proceedings in Physics, vol 188. Springer, Singapore. https://doi.org/10.1007/978-981-10-1926-5_51

[16] Casas, N and Mollon, G and Daouadji, A (2020) Cohesion and Initial Porosity of Granular Fault Gouges control the Breakdown Energy and the Friction Law at the Onset of Sliding. https://doi.org/10.1002/essoar.10504966.1

[17] Soulié, F. and El Youssoufi, M.S. and Cherblanc, F. and Saix, C. (2006) Capillary cohesion and mechanical strength of polydisperse granular materials. The European Physical Journal E 21:349–357. https://doi.org/10.1140/epje/i2006-10076-2

[18] Dorostkar, Omid and Guyer, Robert A. and Johnson, Paul A. and Marone, Chris and Carmeliet, Jan (2018) Cohesion-Induced Stabilization in Stick-Slip Dynamics of Weakly Wet, Sheared Granular Fault Gouge. Journal of Geophysical Research: Solid Earth 123:2115-2126. https://doi.org/10.1002/2017JB015171

[19] Vardoulakis, I. (2002) Dynamic thermo-poro-mechanical analysis of catastrophic landslides. Géotechnique 52:157-171. https://doi.org/10.1680/geot.2002.52.3.157

[20] Rice, James R. (2006) Heating and weakening of faults during earthquake slip. Journal of Geophysical Research: Solid Earth 111. https://doi.org/10.1029/2005JB004006

[21] Gan, Yixiang and Rognon, Pierre and Einav, Itai (2012) Phase transitions and cyclic pseudotachylyte formation in simulated faults. Philosophical Magazine 92:3405-3417. https://doi.org/10.1080/14786435.2012.669062

[22] Mollon, Guilhem and Aubry, Jérôme and Schubnel, Alexandre (2021) Simulating melting in 2D seismic fault gouge. Journal of Geophysical Research: Solid Earth 126, 6. https://doi.org/10.1029/2020JB021485

[23] Idrissi, Hosni and Samaee, Vahid and Lumbeeck, Gunnar and van der Werf, Thomas and Pardoen, Thomas and Schryvers, Dominique and Cordier, Patrick (2020) In Situ Quantitative Tensile Testing of Antigorite in a Transmission Electron Microscope. Journal of Geophysical Research: Solid Earth 125:1-12. https://doi.org/10.1029/2019JB018383

[24] Midi, G D R (2004) On dense granular flows. European Physical Journal E: 14:341-365. https://doi.org/10.1140/epje/i2003-10153-0

[25] Oda, M. and Takemura, T. and Takahashi, M. (2004) Microstructure in shear band observed by microfocus X-ray computed tomography. Géotechnique 54:539-542. https://doi.org/10.1680/geot.2004.54.8.539

[26] Masanobu Oda and Junichi Konishi and Siavouche Nemat-Nasser (1982) Experimental micromechanical evaluation of strength of granular

materials: Effects of particle rolling. Mechanics of Materials 1:269-283. https://doi.org/10.1016/0167-6636(82)90027-8

[27] Zhou, Y.C. and Wright, B.D. and Yang, R.Y. and Xu, B.H. and Yu, A.B. (1999) Rolling friction in the dynamic simulation of sandpile formation. Physica A: Statistical Mechanics and its Applications 269:536-553. https://doi.org/10.1016/S0378-4371(99)00183-1

[28] Alonso-Marroquín, F. and Vardoulakis, I. and Herrmann, H. J. and Weatherley, D. and Mora, P. (2006) Effect of rolling on dissipation in fault gouges. Physical Review E - Statistical, Nonlinear, and Soft Matter Physics 74:1-10. https://doi.org/10.1103/PhysRevE.74.031306

[29] Papanicolopulos, Stefanos Aldo and Veveakis, Emmanuil (2011) Sliding and rolling dissipation in Cosserat plasticity. Granular Matter 13:197-204. https://doi.org/10.1007/s10035-011-0253-8

[30] Ai, Jun and Chen, Jian Fei and Rotter, J. Michael and Ooi, Jin Y. (2011) Assessment of rolling resistance models in discrete element simulations. Powder Technology 206:269-282. https://doi.org/10.1016/j.powtec.2010.09.030

[31] Zhao, Chuang and Li, Chengbo (2016) Influence of rolling resistance on the shear curve of granular particles. Physica A: Statistical Mechanics and its Applications 460:44-53. https://doi.org/10.1016/j.physa.2016.04.043

[32] Iwashita, K. and Oda, M. (1998) Rolling Resistance At Contacts in Simulation of Shear Band. Asce 124:285-292. https://doi.org/10.1061/(ASCE)0733-9399(1998)124:3(285)

[33] Iwashita, Kazuyoshi and Oda, Masanobu (2000) Micro-deformation mechanism of shear banding process based on modified distinct element method. Powder Technology 109:192-205. https://doi.org/10.1016/S0032-5910(99)00236-3

[34] Akira, Murakami and Hide, Sakaguchi and Takashi Hasegawa (1997) Dislocation, vortex and couple stress in the formation of shear bands under trap-door problems. Soils and foundations 37:123-135. https://doi.org/10.3208/sandf.37.123

[35] Zhang, Wangcheng and Wang, Jianfeng and Jiang, Mingjing (2013) DEM-Aided Discovery of the Relationship between Energy Dissipation and Shear Band Formation Considering the Effects of Particle Rolling Resistance. Journal of Geotechnical and Geoenvironmental Engineering 139:1512-1527. https://doi.org/10.1061/(asce)gt.1943-5606.0000890

[36] Tang, Hongxiang and Dong, Yifeng and Chu, Xihua and Zhang, Xing (2016) The influence of particle rolling and imperfections on the formation of shear bands in granular material. Granular Matter 18:1-12. https://doi.org/10.1007/s10035-016-0607-3

[37] Nho, Hien and Nguyen, Gia and Scholtès, Luc and Guglielmi, Yves and Victor, Frédéric (2021) Micromechanics of sheared granular layers activated by fluid pressurization Micromechanics of sheared granular layers activated by fluid pressurization. Geophysical Research Letters, 48, e2021GL093222. https://doi.org/10.1002/essoar.10506504.1

[38] Estrada, Nicolas and Taboada, Alfredo and Radjaï, Farhang (2008) Shear strength and force transmission in granular media with rolling resistance. Physical Review E - Statistical, Nonlinear, and Soft Matter Physics 78:1-11.https://doi.org/10.1103/PhysRevE.78.021301

[39] Yang, Y. and Cheng, Y. M. and Sun, Q. C. (2017) The effects of rolling resistance and non-convex particle on the mechanics of the undrained granular assembles in 2D. Powder Technology 318:528-542. https://doi.org/10.1016/j.powtec.2017.06.027

[40] Liu, Yiming and Liu, Huabei and Mao, Haijun (2018) The influence of rolling resistance on the stress-dilatancy and fabric anisotropy of granular materials. Granular Matter 20, 12. https://doi.org/10.1007/s10035-017-0780-z

[41] Barnett, N. and Rahman, Md Mizanur and Karim, Md Rajibul and Nguyen, H. B.K. (2020) Evaluating the particle rolling effect on the characteristic features of granular material under the critical state soil mechanics framework. Granular Matter 22, 89. https://doi.org/10.1007/s10035-020-01055-5

[42] Maurice Godet (1984) The third-body approach: A mechanical view of wear. Wear 100:437-452. https://doi.org/10.1016/0043-1648(84)90025-5

[43] G. Colas and A. Saulot and C. Godeau and Y. Michel and Y. Berthier (2013) Decrypting third body flows to solve dry lubrication issue – MoS2 case study under ultrahigh vacuum. Wear 305:192-204. https://doi.org/10.1016/j.wear.2013.06.007

[44] Jensen, Richard P. and Bosscher, Peter J. and Plesha, Michael E. and Edil, Tuncer B (1999) DEM simulation of granular media—structure interface: effects of surface roughness and particle shape. International Journal for Numerical and Analytical Methods in Geomechanics 23:531-547. https://doi.org/10.1002/(SICI)1096-9853(199905)23:6¡531::AID-NAG980¿3.0.CO;2-V

[45] Kozicki, J. and Tejchman, Jacek (2011) Numerical simulations of sand behavior using DEM with two different descriptions of grain roughness. Particle-Based Methods II - Fundamentals and Applications.

[46] Mollon, Guilhem and Quacquarelli, Adriana and Andò, Edward and Viggiani, Gioacchino (2020) Can friction replace roughness in the numerical simulation of granular materials ?. Granular Matter 22, 42. https//doi.org/10.1007/s10035-020-1004-5

[47] Wensrich, C. M. and Katterfeld, A. (2012) Rolling friction as a technique for modelling particle shape in DEM. Powder Technology 217:409-417. https://doi.org/10.1016/j.powtec.2011.10.057

[48] Rorato, R. and Arroyo, M. and Gens, A. and Andò, E. and Viggiani, G. (2021) Image-based calibration of rolling resistance in discrete element models of sand. Computers and Geotechnics 131. https://doi.org/10.1016/j.compgeo.2020.103929

[49] Jiang, Ming Jing and Yu, H. S. and Harris, D. (2005) A novel discrete model for granular material incorporating rolling resistance. Computers and Geotechnics 32:340-357. https://doi.org/10.1016/j.compgeo.2005.05.001

[50] Johnson, K.L. (1985) Contact Mechanics. Cambridge University Press, London. https://doi.org/10.1017/CBO9781139171731

[51] Kloss, C. and Goniva, C. and Hager, A. and Amberger, S. and Pirker, S. (2012) Models, algorithms and validation for opensource DEM and CFD-DEM. Progress in Computational Fluid Dynamics 12:140-152. https://doi.org/10.1504/PCFD.2012.047457

[52] C. Thornton and C.W. Randall (1988) Applications of Theoretical Contact Mechanics to Solid Particle System Simulation. Micromechanics of Granular Materials. https://doi.org/10.1016/B978-0-444-70523-5.50023-0

[53] Li, Yanjie and Xu, Yong and Thornton, Colin (2005) A comparison of discrete element simulations and experiments for 'sandpiles' composed of spherical particles. Powder Technology 160:219-228. https://doi.org/10.1016/j.powtec.2005.09.002

[54] Dieterich, James H. (1979) Modeling of rock friction 1. Experimental results and constitutive equations. Journal of Geophysical Research: Solid Earth 84:2161-2168. https://doi.org/10.1029/JB084iB05p02161

[55] Roux, Jean Noël and Combe, Gaël (2002) Quasistatic rheology and the origins of strain. Comptes Rendus Physique 3:131-140. https://doi.org/10.1016/S1631-0705(02)01306-3

[56] Da Cruz, Frédéric and Emam, Sacha and Prochnow, Michaël and Roux, Jean Noël and Chevoir, François (2005) Rheophysics of dense granular materials: Discrete simulation of plane shear flows. Physical Review E - Statistical, Nonlinear, and Soft Matter Physics 72:1-17. https://10.1103/PhysRevE.72.021309

[57] Roux, Jean Noël and Chevoir, François (2010) Analyse dimensionnelle et paramètres de contrôle. In: Modélisation numérique discrète des matériaux granulaires, Radjai F. and Dubois F.. Hermès - L, Paris, pp 223-259

[58] Jaeger, Heinrich M. and Nagel, Sidney R. and Behringer, Robert P. (1996) Granular solids, liquids, and gases 68:1259-1273.https://doi.org/10.1103/RevModPhys.68.1259